DR. WOJCIECH MICHNO (Orcid ID : 0000-0002-3096-3604)

DR. HENRIK ZETTERBERG (Orcid ID : 0000-0003-3930-4354)

DR. JÖRG HANRIEDER (Orcid ID : 0000-0001-6059-198X)

Article type : Original Article

Chemical Imaging of Evolving Amyloid Plaque Pathology and Associated Aβ Peptide Aggregation in a Transgenic Mouse Model of Alzheimer's Disease

Wojciech Michno[1], Patrick Wehrli[1], Silvio Meier[2], Dag Sehlin[2], Stina Syvänen[2], Henrik Zetterberg[1,3,4,5], Kaj Blennow[1,3], and Jörg Hanrieder[1,5]*

1) *Department of Psychiatry and Neurochemistry, Sahlgrenska Academy at the University of Gothenburg, Mölndal, Sweden*
2) *Department of Public Health and Caring Sciences, Uppsala University, Uppsala, Sweden*
3) *Clinical Neurochemistry Laboratory, Sahlgrenska University Hospital, Mölndal, Sweden*
4) *UK Dementia Research Institute at UCL, London, United Kingdom*
5) *Department of Neurodegenerative Disease, Queen Square Institute of Neurology, University College London, London, United Kingdom*

*** Contact:**

Jörg Hanrieder, PhD

Dept. Psychiatry and Neurochemistry, Sahlgrenska Academy at the University of Gothenburg, Mölndal Hospital, House V, Biskopsbogatan 27, SE-43180 Mölndal, Sweden

This article has been accepted for publication and undergone full peer review but has not been through the copyediting, typesetting, pagination and proofreading process, which may lead to differences between this version and the Version of Record. Please cite this article as doi: 10.1111/JNC.14888

jh@gu.se; +46313432377

Abstract

One of the major hallmarks of Alzheimer's disease (AD) pathology is the formation of extracellular amyloid β (Aβ) plaques. While Aβ has been suggested to be critical in inducing and, potentially, driving the disease, the molecular basis of AD pathogenesis is still under debate. Extracellular Aβ plaque pathology manifests itself upon aggregation of distinct Aβ peptides, resulting in morphologically different plaque morphotypes, including mainly diffuse and cored senile plaques. As plaque pathology precipitates long before any clinical symptoms occur, targeting the Aβ aggregation processes provides a promising target for early interventions. However, the chain of events of when, where and what Aβ species aggregate and form plaques remains unclear. The aim of the current study was to investigate the potential of MALDI-IMS as a tool to study the evolving pathology in transgenic mouse models for AD. To that end, we used an emerging, chemical imaging modality – MALDI imaging mass spectrometry – that allows for delineating Aβ aggregation with specificity at the single plaque level. We identified that plaque formation occurs first in cortical regions and that these younger plaques contain higher levels of 42 amino acid-long Aβ (Aβ1-42). Plaque maturation was found to be characterized by a relative increase in deposition of Aβ1-40, which was associated with the appearance of a cored morphology of the plaques. Finally, other C-terminally truncated Aβ species (Aβ1-38 and Aβ1-39) exhibited a similar aggregation pattern as Aβ1-40, suggesting that these species have similar aggregation characteristics. These results suggest that initial plaque formation is seeded by Aβ1-42; a process that is followed by plaque maturation upon deposition of Aβ1-40 as well as deposition by other C-terminally modified Aβ species.

Keywords: MALDI imaging, Alzheimer's disease, beta-amyloid, plaque pathology, transgenics,

Introduction

The molecular basis of Alzheimer's disease (AD) pathology is still under debate. Formation of extracellular amyloid β (Aβ) plaque pathology is the major pathological hallmark of AD and has been identified to be critical in inducing and, potentially, driving AD pathogenesis (Hardy & Higgins 1992). Amyloid plaque pathology develops upon aggregation of distinct Aβ peptides long before any clinical symptoms occur (Braak & Braak 1991, Thal *et al.* 2002). Delineating the earliest events of evolving

Aβ plaque pathology may therefore reveal the most decisive chemical factors that lead to toxic Aβ build up and plaque pathology, respectively that in turn are promising targets for early intervention.

As in situ characterization of early plaque pathology in AD is not possible in living, young patients, initial clues on early plaque formation have been deduced from Down syndrome (DS) patients that exhibit Aβ plaque pathology resembling early plaque pathology in AD (Lemere *et al.* 1996, Ikeda *et al.* 1989, Masters *et al.* 1985). Further, significant work has been presented to identify how plaque formation is initiated by developing genetic mouse models that resemble human plaque pathology (Quon *et al.* 1991, Higgins *et al.* 1994, Games *et al.* 1995, Hsiao *et al.* 1995, Hsiao *et al.* 1996, Sturchler-Pierrat *et al.* 1997). However, it is still under debate what distinct, individual Aβ peptide isoforms, including C- and N-terminal truncations, are involved in early accumulation and seed of Aβ aggregation and plaque formation (McGowan *et al.* 2005, Page *et al.* 2008). into plaques. It is further not fully understood, how the different Aβ species are involved in plaque maturation over age. Theories suggest that seeding and maturation is primary driven by accumulation, aggregation, deposition and N-terminal processing of Aβ42, while Aβ40 has been identified in cored plaques (Iwatsubo *et al.* 1994, Saido *et al.* 1995). It remains however unclear what Aβ peptides influence the structural evolution of the plaque over time, leading to formation of, *e.g.*, diffuse or more densely packed, cored plaques (Nystrom *et al.* 2013, Rasmussen *et al.* 2017, Tycko 2015, Bitan *et al.* 2003) and how this relates to associated neurodegeneration and cognitive deficits (Kuo *et al.* 2001, Kawarabayashi *et al.* 2001).

Delineating the early steps in plaque formation at the scale of individual Aβ peptide species has been limited by the analytical sensitivity and specificity of current biochemical tools used for Aβ imaging, mainly immunohistochemistry (IHC). The advent of novel chemical imaging techniques such as imaging mass spectrometry (IMS) greatly increases the resolution of these events (McDonnell & Heeren 2007, Seeley & Caprioli 2008). In particular, matrix-assisted laser desorption/ionization imaging mass spectrometry (MALDI IMS) is a powerful, emerging technology for comprehensively delineating lipid, peptide and protein localizations in situ, while maintaining high chemical specificity (Hanrieder *et al.* 2015, Hanrieder *et al.* 2013, Michno *et al.* 2018b). In the context of AD, MALDI IMS has been demonstrated to be a powerful tool to measure Aβ peptide pattern *in situ* at single plaque resolution (Carlred *et al.* 2016, Kaya *et al.* 2017, Michno *et al.* 2018a, Michno *et al.* 2019, Michno et al. 2018b, Kakuda *et al.* 2017, Rohner *et al.* 2005, Stoeckli *et al.* 2006, Seeley & Caprioli 2008).

In the present study, we set out to employ MALDI IMS to follow aggregation for individual Aβ peptide species on a single plaque level in a transgenic mouse model of AD ($tgAPP_{Swe}$) that exhibited evolving, heterogenous plaque pathology with age (Lord *et al.* 2006, Lord *et al.* 2011).

The aim of the current study was to investigate the potential of MALDI-IMS as a tool to study the evolving heterogenous plaque pathology in transgenic mouse models for AD. The results show that early plaques at 12 months are more diffuse in nature and contain higher levels of Aβ 1-42. With age, cored plaques are formed upon deposition of Aβ 1-40 and other C-terminal Aβ species, while diffuse plaques at later ages still contain higher levels of Aβ 1-42.

Methods

Chemicals and reagents

All chemicals for matrix and solvent preparation were pro-analysis grade and obtained from Sigma-Aldrich (St. Louis, MO, USA). TissueTek optimal cutting temperature compound was purchased from Sakura Finetek (Cat.#: 4583, AJ Alphen aan den Rijn, The Netherlands). The ddH_2O was obtained from a milliQ purification system (Merck Millipore, Billerica, MA, USA).

Animals and Tissue Collection

Male, transgenic mice with a C57BL/6-CBA-F1 background harboring the Swedish APP mutation ($tgAPP_{Swe}$) (Lord et al. 2006, Lord et al. 2011) were reared in an animal facility at the Swedish Veterinary Institute, Uppsala. This exploratory animal study was not pre-registered. No randomization, blinding and sample calculation was performed. No exclusion criteria were pre-determined and no animals were excluded. Mice at age: 6, 9 months (n=1/group), as well as 12, 18 and 23 months of age (n=3/group) were analyzed in the current study (Figure 1A). A number of with N=3 technical replicates per mouse were analyzed to determine the technical variability.

The animals were reared *ad libitum* in an under a 12/12-hlight/dark cycle (Lord et al. 2006). The animals were anesthetized with isoflurane to minimize suffering and killed by decapitation. The brains were dissected quickly (3 min. postmortem delay) and snap-frozen by immerging the brains in dry ice. All animal procedures were approved by an ethical committee and performed in compliance with national and local animal care and use guidelines (DNr #C17⁄14 at Uppsala University). Frozen sagittal tissue sections (12µm thick) were collected at lateral 1.1-1.35mm using a cryostat microtome (Leica CM 1520, Leica Biosystems, Nussloch, Germany) operating at -18°C. The sections were collected on indium tin oxide (ITO) coated, conducting glass slides (Cat.#: 237001, Bruker Daltonics,

Bremen, Germany), and stored at -80°C. Prior analysis, tissue sections were thawed under vacuum for 1 hour (Figure 1BI).

MALDI IMS Sample Preparation and Matrix Application

For protein imaging, we employed a previously validated protocol for robust peptide and protein imaging (Seeley *et al.* 2008). In detail, tissue sections were subjected to sequential washes of 99.9% EtOH (Cat # V002075; Sigma Aldrich) (60 s), 70% EtOH (30 s), Carnoy's fluid (6:3:1 EtOH/$CHCl_3$/acetic acid) (90 s), 99.9% EtOH (15 s), H_2O with 0.2% TFA (Cat #T6508; Sigma Aldrich) (60 s), and 99.9% EtOH (15 s). As previously reported, tissue was exposed to concentrated formic acid (FA) vapor in order to enhance Aβ peptide signal (Kakuda et al. 2017), which however compromises detection of other intact protein signals. 2,5-Dihydroxy-acetophenone (2,5-DHA) was used as matrix compound (Cat.#: D107603, Sigma Aldrich) and applied using a TM Sprayer (HTX Technologies, Chapel Hill, NC, USA) (Figure 1BII). A matrix solution of 15 mg/mL 2,5-DHA in 70% ACN/2%CH_3COOH/2%TFA was sprayed onto the tissue sections using the following instrumental parameters: nitrogen flow (10 psi), spray temperature (75°C), nozzle height (40 mm), eight passes with offsets and rotations, and spray velocity (1000 mm/min), and isocratic flow of 100µL/min using 70% ACN as pushing solvent. Following matrix deposition, the preparations were recrystallized as described previously (Yang & Caprioli 2011). Here, the slides were mounted with copper tape on the inner side of the top lid of a Petri dish (100 mm diameter×15 mm deep, Cat # 75845-546, VWR, Radnor, PA) with a filter paper pipetted with 5% methanol and placed on the lower part of the dish. The glasses were closed and placed in an oven at 85°C for 3 min.

MALDI imaging MS

MALDI-IMS was performed on a MALDI TOF/TOF UltrafleXtreme mass spectrometer (Bruker Daltonics, Bremen, Germany) equipped with SmartBeam II Nd:YAG/355 nm laser. Protein MS data were acquired over a mass range of 2–20 kDa, running in linear positive mode (Figure 1BIII). The apparent mass resolution was $m/\Delta m$=1000 (FWHM) at m/z 4515, which was well in line with the reference values for this mass range provided by the manufacturer. A number of 50 laser shots/raster spot were acquired at 1 kHz laser repetition rate. The laser beam focus was set to 'small', resulting in a lateral resolution of 25 µm. Image data were reconstructed; total ion current (TIC) normalized and visualized using the Flex Imaging software (v.3.0, Bruker Daltonics). External

calibration was performed from calibrant solution spots (Protein Calibration Mix 1, Bruker Daltonics) that were placed adjacent to the tissue slides.

Statistical Analysis: Data Processing and Image Data Segmentation

Prior to analysis, all spectra were calibrated externally using the batch-processing function in Flex Analysis (v 3.0, Bruker Daltonics). Image analysis of the IMS data was performed in SciLS (v2015, Bruker Daltonics). Spatial segmentation using bisecting k-mean clustering was performed in order to identify characteristic proteins distribution patterns and to aid in region of interest (ROI) identification yielding clusters also annotated as pseudo-objects that localized to plaque feature. ROIs in aligned imaging MS data were annotated, based on the pseudo-objects, i.e. clusters, obtained through segmentation, the average MS spectra of the annotated ROIs were exported as *.csv files from FlexImaging. All ROI data (10-15 plaques per subtype per region) were imported into Origin (v. 8.1, OriginLab, Northhampton, MA, USA) and peaks were detected on average spectra of each ROI using the implemented peak analyzer function. The determined bin borders for peak integration were exported as tab-delimited text file followed by binning of all ROI average spectra using an in-house-developed R script (peak-bin), as described previously (Hanrieder *et al.* 2011). The extracted average peak data from the different plaque-ROI were subjected to log2 transformation to make variation similar across orders of magnitude and to achieve a more normal distribution of the data. This was followed by univariate statistical comparisons of the respective plaque subtypes (diffuse and cored) for each animal, for a given age and region by means of paired, two tailed t-test ($p<0.05$) using Prism (v.7, GraphPad, San Diego, CA, USA). The technical variation as a consequence of sample preparation was determined by evaluating N=3 replicate sections obtained from the same animal and prepared and analyzed individually. Here spectral data of cortical plaque ROI were compared and gave an RSD of 11%. Further, Stability of Sample Preparation was determined through cross evaluation of plaque free control areas by plotting all intensity values for each mass signal in between two consecutive experiments on technical replicates from the same mouse brain. Plots for experiment pairs show linearity of the relation between experiments verifying the stability and reproducibility of measurements (Supplemental Figure 1).

Aβ plaque isolation, Aβ immunoprecipitation and MS/MS verification

Laser microdissection pressure catapulting (LMPC) was done using a PALM Microbeam LMPC microscope (Zeiss) equipped with a 355 nm pulsed UV-laser. The isolated amyloid aggregates were

extracted with 50µL of 99% formic acid. The samples were then neutralized to pH 7 using 0.5M Tris and Aβ peptides were then purified through immunoprecipitation using Aβ-specific antibodies Aβ 1-16 (6E10, RRID: AB_2564652) and Aβ 17.24 (4G8, RRID: AB_662812; both Signet Laboratories, BioLegend, San Diego, CA, USA)], coupled to magnetic Dynabeads M-280 Sheep Anti-Mouse (RRID:AB_2783009, Thermo Fisher, Carlsbad, CA, USA) as described previously (Rasmussen et al. 2017, Portelius *et al.* 2007). The supernatant was collected and dried through lyophilization. Mass spectrometric comparison of the samples was performed using a MALDI TOF/TOF UltraFleXtreme instrument (Bruker Daltonics) as described previously using α-Cyano-4-hydroxycinnamic acid (CHCA) as matrix (Cat.#: C8982, Sigma Aldrich). Further, to verify the identity of the observed peptides, an LC-MS/MS analysis, was carried out using a Q Exactive quadrupole-orbitrap hybrid mass spectrometer equipped with a heated electrospray ionization source (HESI-II) (Thermo Scientific, Waltham, MA, USA) and UltiMate 3000 binary pump, column oven, and autosampler (Thermo Scientific), as previously described (Pannee *et al.* 2016), but with the Q Exactive operated in data dependent mode. Briefly, the resolution settings were 70,000 and target values were 1×10^6 both for MS and MS/MS acquisitions. Acquisitions were performed with 1 micro scan/acquisition. Precursor isolation width was 3 m/z units and ions were fragmented by so-called higher energy collision induced dissociation (HCD) at a normalized collision energy (NCE) of 25. Spectra were deconvoluted using Mascot Distiller before submission to database search using the Mascot search engine (both Matrix Science) as described previously (Brinkmalm *et al.* 2012). The MS/MS spectra were searched toward the SwissProt database containing the mutant human APP sequence using the following search parameters: taxonomy; Homo sapiens, precursor mass ± 20 ppm; fragment mass ± 0.05 Da; no enzyme; no fixed modifications; variable modifications including deamidated (NQ), Glu->pyro-Glu (N-term E), oxidation (M); instrument default.

Fluorescent amyloid staining

Following MALDI analysis, fluorescent plaque imaging was performed using luminescent conjugated oligothiophene (LCO) amyloid probes (Klingstedt *et al.* 2011) as previously described, with few modifications (Michno et al. 2018a). Shortly, sections were rinsed in absolute EtOH for 60s, fixed in 99.9%EtOH at -20°C for 8 min, 70%EtOH at -20°C for 30sec, 70%EtOH at RT for 30sec, and stored in PBS prior to staining. For amyloid staining, 30 minutes incubation with heptamer-formyl thiophene acetic acid (h-FTAA) (1.5µM) was used (Klingstedt et al. 2011, Nystrom et al. 2013). Following staining tissue was washed three times 1 min in PBS (*Cat.#:* P9416, Sigma Aldrich) , and dried at

RT. Overview imaging was performed using a wide-field microscope (Axio Observer Z1, Zeiss, Jena, Germany) with a Plan-Apochromat 10x/0.3 DIC objective and a 38 HE-AF488 filter (Ex: BP 479/40; Em: BP 525/50). Fluorescent images were imported into the SciLS software and aligned with the imaging data.

Immunohistochemistry

For antibody-based staining, tissue was fixated with 4% PFA in PBS for 20 min. Sections underwent antigen retrieval in citrate buffer (25mM, pH 7.3) at 86°C for 20 min followed by treatment with 70% formic acid for 5min at RT. Endogenous peroxidase activity was blocked with peroxidase blocking reagent (Cat.#: S202386-2, DAKO, Agilent, Santa Clara, CAQ, USA)) for 20min followed by 3% hydrogen peroxide (Cat.#: 7722-84-1, Sigma Aldrich) in PBS for 20min. Sections were permeabilized with 0.4% Triton X-100 (Cat.#: T8787, Sigma Aldrich) in PBS for 30 minutes. Unspecific binding was blocked with 5% normal goat serum (Cat.#: S-1000, Vector Laboratories Inc, Burlingame, CA, USA.) for 1h. The sections were incubated with custom-made primary polyclonal anti-Aβ40 and anti-Aβ42 antibodies (Agrisera AB, Vännäs, Sweden) in PBS-TWEEN® 20 (0,1%) (Cat.#: P9416, Sigma Aldrich) at 4°C overnight. The secondary biotinylated goat anti-rabbit antibody (Cat.#: BA-1000, Vector Laboratories) was applied for 2h at RT followed by 1h incubation with avidin/biotin complex (Cat.#: PK-7100, Vector Laboratories). The visualization of the staining was performed with the SK-4800 peroxidase substrate kit (Cat.#: SK-4800, Vector Laboratories) for 20 seconds and mounted with DPX mounting media (Cat.#: 06522, Sigma Aldrich).

Results

MALDI IMS and Multivariate Image Data Analysis Reveal Chemical Heterogeneity of Amyloid Plaque Pathology

We here set out to follow aggregation for Aβ peptide species on a single plaque level in a transgenic tgAPP$_{SWE}$ mice. For this we analyzed the Aβ composition of single plaques, in relation to plaque morphology, at different time points. Here the aim was to identify the relation of distinct Aβ signatures associated with heterogeneous plaque formation.

We employed MALDI imaging to probe the distinct Aβ peptide composition of evolving amyloid plaque pathology in 6-, 9-, 12-, 18-, and 23-month-old tgAPP$_{SWE}$ mice. Following data acquisition, spatial segmentation using bisecting k-means cluster analysis of the multivariate IMS data was performed in order to reveal a histologically relevant localization pattern associated with plaque

pathology. For 6- and 9-month-old mice, no plaque pathology was observed in general (Supplemental Figure 2). For 12-month old mice, plaque-like features were detected in the somatomotor cortex of all animals but not in the somatosensory cortex and hippocampus (Figure 2A.I-D.I). The associated chemical species was contained in the derived pseudo-objects.

For 18-month-old (Figure 2A.II-D-II) and 23-month-old (Figure 2A.III-D.III, Supplemental Figure 2) animals, pronounced plaque deposition was observed in the somatomotor cortex, somatosensory cortex and the hippocampus. Interestingly, for all mice at 18 and 23 months, spatial segmentation revealed two prominent clusters associated with these plaque features, suggesting both a distinct chemical but possibly also structural heterogeneity among these deposits. Therefore, to verify the identity of the pseudo-objects identified through spatial segmentation as amyloid plaques, subsequent fluorescent amyloid staining of the MALDI IMS-analyzed tissue was performed. Careful alignment of brightfield tissue scans with the fluorescent images, and thereafter the cluster images obtained through spatial segmentation, revealed the pseudo-objects that matched the amyloid-positive deposits (Figure 3A.I-AIV). Further inspection of the individual pseudo-objects in respective anatomical regions, including somatomotor cortex (Figure 3B.I-BIV), somatosensory cortex (Figure 3C.I-C.IV) and hippocampus (Figure 3D.I-DIV), revealed the presence of a core to be associated with one of the plaque pseudo-objects (green), while no core but rather diffuse fibrillary structures to underlie the other (yellow). Finally, spatial correlation analysis of the m/z peaks with the clusters present in 12-, 18-, and 23-month old animals (Figure 4A.I-A.III) displayed predominant localization of different individual mass peaks at m/z 4000-4600 across the anatomical regions. Putative assignment based on intact mass identified these peaks to corresponding to differentially C-terminally truncated Aβ peptides (Figure 4B.I-B.III).

None of the detected peptides were post-translationally modified, which are generally low abundant in this mouse model and could not be detected due to limited sensitivity of IMS over analysis of whole tissue extract (Wittnam *et al.* 2012).

To further validate the peptide identities, we performed laser microdissection of amyloid positive plaque features followed by immunoprecipitation and peptide identification using liquid chromatography hyphenated to high resolution mass spectrometry (LC-MS). Here we identified Aβ1-42 (Figure 4C.I-C.III) and Aβ1-40 (Figure 4D.I-D.III), but also Aβ1-39 (Figure 4E.I-E.III), Aβ1-38 (Figure 4.FI-F.III), and Aβ1-37 (Figure 4G.I-G.III), to underlie the diverse pseudo-objects (Supplemental Table 1, Supplemental Figure 3A-E).

Evolving Amyloid Plaque pathology is reflected by an increased Aβ1-40/Aβ1-42 ratio

In order to identify the chemical difference between the individual pseudo-objects identified in k-means cluster analysis that were corresponding to Aβ plaques, those objects, were annotated as plaque type specific regions of interests (ROI) followed by evaluating ROI deduced IMS spectral data through univariate statistical analysis.

Here, plaques with a primarily diffuse structure present in the somatomotor cortex of 12-month-old mice (Figure 5A.I), show equal amounts of Aβ1-42 (Figure 5B.I) and Aβ1-40 peptides (Figure 5C.I) in equivalent amounts, clearly seen in the overlay image (Figure 5D.I). In contrast, for the 18-, and 23-month-old mice, we identified the Aβ1-42 peptide (Figure 5B.II-B.V) primarily in plaques belonging to the pseudo-object that appeared to be associated with the diffuse plaques (Figure 5A.III, A.V). In contrast, Aβ1-40 peptide (Figure 5C.II-C.V) was found to be associated with a pseudo-object that corresponded to the cored plaques (Figure 5A.II, A.IV).

Investigation of the overlay images (Figure 5D.II-D.V) revealed the Aβ1-42 to also be present in the periphery of the cored plaques. These data were further validated through IHC, showing similar distribution patterns of Aβ1-42 and Aβ1-40 for the different plaque morphologies and the different ages (Supplemental Figure 4).

Further, given this characteristic deposition pattern of Aβ1-42 and Aβ1-40, we compared the Aβ1-40/1-42 across the diffuse and cored plaque populations in somatomotor cortex, hippocampus, and somatosensory cortex, for the respective ages.

Here, plaques in the somatomotor cortex of 12-month old animals displayed an intermediate peptide profile. Specifically, at 12 months, Aβ1-40/1-42 was two-fold higher in these plaques as compared to diffuse plaques at 18-, and 23-months. Further, at 18-, and 23-months, the Aβ1-40/1-42 ratio was four-fold higher in cored plaques as compared to diffuse plaques (Figure 5E.I). This relative increase of Aβ1-40/1-42 in cored plaques at 18-, and 23-months was based on a 2-fold increase of Aβ1-40 in cored plaques at this age and a 2-fold decrease in Aβ1-42 peptide. The relative decrease in Aβ1-40/1-42 as compared to the diffuse plaques at 18-, and 23-months was based on a 2-fold increase of Aβ1-42 in diffuse plaques. For plaques in the hippocampus and somatosensory cortex, Aβ1-40/1-42 peptide ratio was also four times higher in cored plaques than in diffuse plaques both in both 18-, and 23-month-old animals (Figure 5E.II-E.III).

For the individual signal intensites of Aβ1-42 and Aβ1-40, the results show that the levels of Aβ1-42 in diffuse plaques were two times higher than in cored plaques for both 18-, and 23-month-old animals (Supplemental Figure 5A). In contrast, the ion signal of Aβ1-40 was more than two times

higher, in cored plaques for both 18-, and 23-month-old animals and across all regions (Supplemental Figure 5B). No significant differences were found in either Aβ1-42, Aβ1-40 or the Aβ1-40/1-42 peptide ratios between regions and between 18-, and 23-month-old animals. Further, Aβ1-42 did not correlate with the Aβ1-40 in neither the diffuse, nor cored deposits (Supplemental Figure 5C). As both IMS and IHC analyses could represent solely the surface peptide distribution of the various Aβ species we performed laser microdissection of individual plaque morphotypes with subsequent immunoprecipitation (IP) and MALDI MS analysis. Here, similar trends of relative Aβ 1-40 deposition in cored plaques were observed with an relative higher ratio of Aβ1-40/1-42 in cored plaques thereby further validating the IMS data (Supplemental Figure 6).

C-terminally Truncated Aβ Peptides are Associated with Heterogeneous Plaque Morphology

Following image analysis, the spatial correlation analysis of the m/z peaks with the pseudo-objects, revealed Aβ plaques to consist of several shorter Aβ peptides with C-terminal truncations. Here, an intermediate mix of both Aβ1-40 and Aβ1-42 was observed in early, cortical, plaques at 12 months (Figure 6A.I, Supplemental 4A,B), while at 18 and 23 months, a predominance of Aβ1-40 was observed for cored plaques (Figure 6A.II, A.IV, Supplemental Figure 4C,E) along with higher levels of Aβ1-42 in diffuse plaques (Figure 6A.III, A.V, Supplemental Figure 4D,F).

In addition to the full length peptides, the shorter C-terminally truncated Aβ species (Aβ1-39, Figure 6C.I-V; Aβ1-38, Figure 6D.I-V; and Aβ1-37, Figure 6E.I-V) displayed distinct distribution patterns in diffuse and cored plaques. Aβ1-39 (Figure 6C.V), Aβ1-38 (Figure 6D.V), and Aβ1-37 (Figure 6E.V) were consistently observed in early plaques in somatomotor cortex of the 12-month-old animals. In contrast, in the older mice (particularly so in 23-month old mice), Aβ1-39 appeared to localize mainly to the cored plaques (Figure 6C.II, C.IV), not to diffuse (Figure 6C.III, C.V). Aβ1-38, exhibited a similar pattern, but localization to cored plaques (Figure 6D.II, D.IV) was much more pronounced; the peptide was not detectable in diffuse plaques (Figure 6D.III, D.V). This pattern was very similar to that of Aβ1-40 (Figure 6B.I-V), described earlier. Finally, Aβ1-37 was not reliably detected in plaques from older animals (Figure 6E.II-V).

Given the characteristic single ion distributions for these peptides, we evaluated the corresponding ion signal from individual regions of interests (ROI), which were previously outlined based on the pseudo-objects. In 23-month old mice, Aβ1-39 was consistently higher in cored as compared to diffuse deposits in all of the somatomotor cortex (Figure 6F.I), hippocampus (Figure 6F.II) and

somatosensory cortex (Figure 6F.III). Further the difference between cored and diffuse plaques was also present in the somatomotor cortex for the 18-month old animals.

In agreement with the single ion images, the Aβ1-38 was significantly more abundant in cored as compared to diffuse plaques, for both the 18-, and 23-month-old animals, also in all of the somatomotor cortex (Figure 6G.I), hippocampus (Figure 6GF.II) and somatosensory cortex (Figure 6G.III). In contrast, the signal intensity of Aβ1-37 did not appear to differ between diffuse and cored plaques in 18-, and 23-month-old animals, for either of the anatomical regions (Figure 6H.I-H.III). Finally, we evaluated the similarities in localization patterns between the shorter C-terminally truncated peptides and Aβ1-40, respective Aβ1-42 for cored and diffuse plaques across regions. Here, regression analysis revealed a positive correlation between Aβ1-39 and Aβ1-40 for the cored plaques (Figure 6F.IV), but not among the diffuse ones (Figure 6F.V). Further, Aβ1-38 had strong correlation with the signal of Aβ1-40, across both the cored (Figure 6G.IV) and diffuse (Figure 6G.V) plaques. In contrast, no correlation was found between Aβ1-37 and Aβ1-40 for either of the plaque populations (Figure 6H.IV, H.V). None of the peptides correlated significantly with Aβ1-42, although a clear positive trend was observed for Aβ1-38 and Aβ1-42 in cored plaques.

Discussion

In the present study, we set out to employ MALDI Imaging mass spectrometry to follow aggregation for individual Aβ peptide species on a single plaque level in a transgenic mouse model of AD ($tgAPP_{SWE}$). The aim was to investigate the potential of MALDI-IMS as a tool to study the evolving pathology in transgenic mouse models for AD. This is important as heterogenous plaque pathology is both characteristic for sporadic and familial AD as well as for Downs syndrome (Ikeda et al. 1989, Lemere et al. 1996). The here used $tgAPP_{SWE}$ mouse model was chosen to study evolving Aβ plaque pathology, as these displays heterogenous plaque pathology with an initial formation of smaller cored Aβ deposits at 10-12 months, followed by further exponential deposition of cored, and some diffuse plaques until full-blown pathology is reached at 18 months, (Philipson *et al.* 2009, Iwatsubo et al. 1994, Kuo et al. 2001). Our results show that for this mouse model plaque pathology precipitates in cortical regions where earlier formed plaques contain higher levels of Aβ1-42. This changes gradually upon plaque maturation over time; more mature plaques were found to be characterized by increased abundance of Aβ1-40. These data suggest that initial plaque formation is seeded by Aβ1-

42 and followed by plaque maturation upon deposition of Aβ1-40, as well as other C-terminally modified Aβ species i.e. Aβ1-38, Aβ1-39.

In line with these data, plaque pathology associated deposition of multiple C-terminally truncated peptides (Aβ1-37, Aβ1-38, Aβ1-39 and Aβ1-40) was previously described for familial AD (FAD) cases with the Swedish APP mutation (Reinert *et al.* 2014, Reinert *et al.* 2016) as well as in various transgenic mouse models carrying this mutation (Reinert et al. 2016, Hsiao et al. 1996, Kawarabayashi et al. 2001, Kuo et al. 2001).

IHC studies did not identify any Aβ plaque pathology in young 6-, and 9-month- old mice in AD models based on the Swedish mutation (Philipson et al. 2009, Iwatsubo et al. 1994, Kuo et al. 2001). Therefore, we did not expect to find any Aβ plaque pathology at these ages, and consequently analyzed only one animal for each of those ages. Indeed, in agreement with other studies, no Aβ signal was observed in these mice (Philipson et al. 2009, Iwatsubo et al. 1994, Kuo et al. 2001). Aβ plaque deposition, although sparse, was first observed in 12-month-old mice (primarily in the somatomotor cortex). This is consistent with previous studies on tgAPP$_{SWE}$ mice, where the first signs of cored Aβ plaque pathology did develop in the neocortical regions (Sturchler-Pierrat et al. 1997, Kawarabayashi et al. 2001, Kuo et al. 2001, Philipson et al. 2009). This is also consistent with the tissue specificity of the promoter giving the highest expression of human APP in the cortical brain region (Howlett 2011, Lord et al. 2006).

Spatial image segmentation, based on the chemical signature present in the MALDI IMS data sets, also revealed two key pseudo-objects being present in the 12-, 18-, and 23-month-old animals. Subsequent fluorescent amyloid staining of the MALDI IMS analyzed tissue identified these pseudo-objects to correspond to Aβ plaque, which either possessed a prominent core, or were diffuse in nature. Surprisingly, the presence of only two pseudo-objects across the three analyzed anatomical regions, (MO-ctx, SS-ctx, HIP), suggested that except differences between these plaque types, only minor differences were present between the Aβ plaques in these regions. The primary chemical differences was therefore attributed to morphology i.e. cored and diffuse plaques and not the area of plaque formation.

The tgAPP$_{SWE}$ mouse model appeared to exhibit primarily C-terminally truncated peptides. Here, as previously shown through IHC, Aβ1-40, Aβ1-39, Aβ1-38, and Aβ1-37 were observed along besides the commonly recognized Aβ1-42 (Reinert et al. 2016). In agreement with the previous observations in tgAPP$_{ArcSwe}$ mice, Aβ1-40 was found to be the primary peptide (Carlred et al. 2016).

No consistent changes of N-terminally truncated Aβ peptide were detected across all the mice, presumably due to their very low abundance.

With respect to the associated chemistry, the two pseudo-objects corresponding to the cored and diffuse plaques differed primarily by the dominant presence of the Aβ1-40 in the cored plaques, and that of Aβ1-42 in the diffuse Aβ deposits. Interestingly, while the ratio of the Aβ1-40/1-42 peptide ratio was roughly four-fold higher in cored as compared to diffuse plaques in 18-, and 23-month-old animals, plaques present in the 12-month-old mice displayed an Aβ1-40/1-42 peptide ratio that was intermediate to that of those two plaque subtypes in older animals. This suggests that while the plaques in the 12-month-old mice might be sparse and not exhibit an as dense center as cored plaques in 18-, and 23-month old mice, they are more mature than the diffuse plaques in the older animals.

This could be a result of a localized “sink effect”, where plaque growth is based on the presence of the Aβ peptides available in the proximity of the plaque seed. In the presence of only few plaque seeds, Aβ1-40 and other peptides aggregate quickly into the newly formed plaques. In older mice, however, where the pathology is far more developed, new plaque seeds are formed at a higher rate, resulting in local regions that may be Aβ1-42-saturated, leading to a more heterogeneous Aβ plaque population with more diffuse plaques. Along this line, in the 18-month-old animals the significant difference in the Aβ1-40/1-42 ratio can be attributed primarily to the increased abundance of Aβ1-40 in cored plaques, as Aβ1-42, even though more abundant in diffuse plaques, is not significantly different. In contrast, in the 23-month-old animals, not only Aβ1-40, but also Aβ1-42 differed significantly between the cored and diffuse plaques. Overall, this would suggest that the process of an individual plaque maturation, as represented by core formation, is accompanied by deposition of C-terminally truncated peptides, with Aβ1-40 being the key peptide. Indeed, previous conventional immunohistological assessment of transgenic APP mice showed prominent Aβx-40 immunoreactivity for plaque cores, whilst Aβx-42 was found to stain mostly the periphery, as well as diffuse deposits (Kuo et al. 2001, Philipson et al. 2009, Kawarabayashi et al. 2001). Our study corroborates these findings, while adding further support with respect to molecular specificity and resolution.

The differential localization pattern and aggregation dynamics of Aβ1-42 and Aβ1-40 can be attributed to the propensity of Aβ1-42 to rapidly convert from monomers to form oligomers and then fibrils (Ahmed *et al.* 2010, Esbjorner *et al.* 2014). The higher levels of Aβ1-42 in diffuse hippocampal deposits could therefore reflect an essential role of these peptide species in the initial seeding of Aβ aggregation and plaque formation.

In further support of this, we observed shorter Aβ peptides (Aβ1-37, 1-38, 1-39) to be primarily present in cored but not diffuse deposits in older mice. Interestingly, similar to Aβ1-40, Aβ1-38 differed between cored and diffuse plaques, across all the three regions, for both 18-, and 23-month-old mice. The longer Aβ1-39 peptide, while clearly elevated in all cored plaques, was found to be changed in 23-month-old mice, as well as in the somatomotor cortex of 18-month-old mice. Both Aβ1-38 and Aβ1-39 correlated with Aβ1-40, and with one another, across all cored deposits. Further, Aβ1-38 was found to correlate with Aβ1-40 in diffuse plaques, while no correlation was found between Aβ1-37 and any of the other peptides.

Mechanistically, formation of the shorter C-terminally peptides: Aβ1-37, Aβ1-38, and Aβ1-39, is considered a result of sequential processing of the APP C-terminal fragment (β-CTF) by γ-secretase (Nunan & Small 2000). Recent studies have shown that prior to this processing, β-CTF is initially subject to ε-cleavage either at Thr-48 or Leu-49, with consecutive loss of tripeptides, resulting in preferential production of Aβ1-40 from Leu-49, or Aβ1-42 from the Leu-49 cleavage (Chen *et al.* 2014, Funamoto *et al.* 2004). However, cleavages at every fourth, fifth and sixth amino acid have also been proposed (Matsumura *et al.* 2014). Yet, while differential processing is possible, formation of Aβ1-38 has been shown to be independent of Aβ1-42 (Czirr *et al.* 2008, Page et al. 2008), which is also in line with our observation. Overall, this suggests that these shorter C-terminally truncated Aβ variants co-aggregate with Aβ1-40 within a plaque upon plaque maturation rather than being formed on site from pre seeded 1-42.

It is important to highlight that the Swedish mutation in the mouse model for AD studied here, is a rather unique mutation that is outside of the N-terminus of the Aβ peptide. Therefore, it results in an increase of total Aβ. In difference, the majority of AD associated APP mutations are present either within the Aβ-sequence, or C-terminally. This leads to either increase in aggregation propensity of the peptides, or an altered Aβ42/40 ratio. Therefore, while outside of the scope of this study, it would be highly relevant to perform similar analysis in other mouse models with intra Aβ or C-terminal mutations (e.g. Arctic and London). Yet, the majority of the AD cases are sporadic, and are believed to be caused by a misbalance in the general Aβ production or clearance. Therefore, in terms of APP mutations the Swedish mutation could be argued to actually be the most suited mutation to model sporadic AD.

In addition to Aβ plaques, human AD pathology is associated with presence of neurofibrillary tangles composed of hyperphosphorylated tau protein. Therefore, analysis of a mouse model that

recapitulates both of these pathologies (e.g. 3xTg, also including a presenilin-1 mutation) could potentially be more relevant due to the potential interplay between Aβ and tau (Nisbet *et al.* 2015).

In summary, we used MALDI imaging MS in tgAPP$_{SWE}$ mice of different ages to delineate evolving amyloid pathology at the peptide scale on the single plaque level. We identified that plaque formation occurs first in cortical regions and that these newly formed plaques contain higher levels of Aβ1-42. Plaque maturation over time was found to be characterized by increased deposition of Aβ1-40. These data suggest that initial plaque formation is seeded by Aβ1-42 and followed by plaque maturation upon deposition of Aβ1-40, as well as other C-terminally truncated Aβ species through secondary nucleation.

Involves human subjects:
If yes: Informed consent & ethics approval achieved:
=> if yes, please ensure that the info "Informed consent was achieved for all subjects, and the experiments were approved by the local ethics committee." is included in the Methods.

ARRIVE guidelines have been followed:
Yes
=> if it is a Review or Editorial, skip complete sentence => if No, include a statement: "ARRIVE guidelines were not followed for the following reason:
"
(edit phrasing to form a complete sentence as necessary).
=> if Yes, insert "All experiments were conducted in compliance with the ARRIVE guidelines." unless it is a Review or Editorial

Conflicts of interest: none
=> if 'none', insert "The authors have no conflict of interest to declare."
=> otherwise insert info unless it is already included

Acknowledgements

The Swedish Research Council VR (#2014-6447, #2018-02181 JH; #2018-02532, HZ; #2017-00915, KB , #2017-02413 SS, #2018-02715 DS), Alzheimerfonden (JH, KB, SS, DS), Alzheimer Research UK (JH), Hjärnfonden (HZ, KB, SS, DS), the Knut and Alice Wallenberg Foundation (HZ), the

European Research Council (#681712 HZ), Swedish State Support for Clinical Research (#ALFGBG-720931 HZ), Åhlén-Stiftelsen (JH, SS, DS), Åke Wiberg Foundation (JH, DS), Stiftelsen Gamla Tjänarinnor (JH, KB, WM, DS), Stohnes Stiftelse (JH, WM, DS), Torsten Söderberg Foundation (KB, SS), Demensfonden (WM, PW) and Frimurarestiftelsen (HZ) are acknowledged for financial support. We are grateful to Prof. Lars N.G. Nilsson, who developed and characterized the mouse model.

Materials availability statement

Custom made materials are available upon reasonable request; please direct requests to Uppsala University directly.

Conflict of interest disclosure: HZ has served at scientific advisory boards for Roche Diagnostics, Samumed, CogRx and Wave, and is a co-founder of Brain Biomarker Solutions in Gothenburg AB, a GU Ventures-based platform company at the University of Gothenburg (all unrelated to the submitted work). The other authors declare no conflict of interest.

Abbreviations

AD – Alzheimer's Disease

Aβ - Amyloid-β

APP - Amyloid precursor protein

hFTAA - heptamer-formyl thiophene acetic acid

HIP – hippocampus

IHC – immunohistochemistry

IP - immunoprecipitation

LC-MS – liquid chromatography mass spectrometry

LCO – luminescent conjugated oligothiophenes

LMPC laser microdissection pressure catapulting

MALDI IMS - matrix-assisted laser desorption/ionization imaging mass spectrometry

MO – somatomotor cortex

ROI – region of interest

RRID, Research Resource Identifier (see scicrunch.org)

SS – somatosensory cortex

tgAPP$_{Swe}$ – transgenic mice harboring the Swedish APP mutation

TIC – total ion current

TOF – time of flight

Figure Legends

Figure 1. Schematic outline of the study. (A) Transgenic mice (tgAPP$_{SWE}$) at age: 6, 9 months (n=1/group), as well as 12, 18 and 23 months of age (n=3/group) were analyzed in the current study. Animals were anesthetized with isoflurane and killed by decapitation followed by brain isolation and snap freezing. (B.I) Cryosections were collected followed by matrix application (B.II) and MALDI imaging analysis (B.III).

Figure 2. Spatial segmentation for ROI Annotation of MALDI-MS imaging data from tgSwe animals of different ages. Hippocampus (HIP), somatosensory cortex (SS) and somatomotor cortex (MO) of (A.I) 12-month-, (A.II) 18-month-, and (A.III) 23-month-old APP transgenic mice harboring the Swedish APP mutation were chosen for the MALDI-MS imaging analysis. Follow-up spatial segmentation of imaging MALDI-MS data, and its partial overlay with the anatomical regions revealed, (B.I) rare in 12-month-old, but prominent in (B.II) 18-month, and (B.III) 23-month-old mice, plaque-like features being present in the those regions for respective ages. (C) Investigation of (C.I-III) spatial segmentation images and corresponding (D.I-III) dendrograms for respective ages, revealed presence of two prominent plaque-like clustering features. Scalebar: 1mm.

Figure 3. Localization of plaque-like pseudo-objects to distinct Aß stained structures. Sample Aß plaque rich anatomical brain region as seen in (A.I) partial overlay of tissue scan and amyloid postive stained image, (A.II) amyloid staining, (A.III) partial overlay of segmentation image and amyloid staining, and (A.IV) image segmentation, demonstrate co-localization of green pseudo-objects to more aggregated (cored) and yellow to less aggregated (diffuse) Aß plaque structures. Zoom of (B.I-IV) ROI 1 - cored (left arrow) and diffuse (right arrow) plaques in somatomotor cortex, (C.I-IV) ROI 2 - cored plaques (arrows) in somatosensory cortex, and

(D.I-IV) diffuse plaques (arrows) in hippocampus, as seen in above described image setup. Scalebar A: 1mm, B-D: 100µm.

Figure 4. Single ion images of different Aß peptides present in plaques across different ages. (A.I-III) Segmentation of sample IMS data from (A.I) 12-, (A.II) 18-, and (A.III) 23-month-old animals display localization of Aß plaque corresponding pseudo-objects. (B.I-III) Partial overlay of tissue scan and the overall major Aß1-40 peptide signal underlying the plaque pseudo-objects for animals of respective ages. Single ion images for (C.I-III) Aβ1-42, (D.I-III) Aβ1-40, (E.I-III) Aβ1-39, (F.I-III) Aβ1-38, (G.I-III) Aβ1-37 peptides across ages. Scalebar 1mm.

Figure 5. Single plaque analysis suggests Aβ1-40/Aβ1-42 ratio to be a critical factor associated with formation of highly aggregated (cored) Aβ deposits. Fluorescent amyloid staining from MO cortex demonstrating (A.I) an intermediate plaque in 12-month-old mouse, (A.II) a cored plaque in 18-month-old mouse, (A.III) a diffuse plaque in 18-month-old mouse, (A.IV) a cored plaque in 23-month-old mouse, and (A.V) a diffuse plaque in 23-month-old mouse. Plaques in the 12-month-old mice appeared structurally similar to the diffuse plaques in older mice. Single ion images of (B.I-V) Aβ1-42 peptide and (C.I-V) Aβ1-40 for the respective plaques types and mice ages listed above. Overlay images of the Aβ1-40 and Aβ1-42 peptide signal showed clear predominance of Aβ1-40 peptide in (D.II, D.IV) cored plaques and of Aβ1-42 in (D.III, D.V) diffuse plaques of the 18- and 23-month-old mice. The (D.I) plaque of a 12-month-old mouse displayed a much more mixed peptide profile, as seen in the composite yellow color. Scatter plot of the average Aβ1-40/Aβ1-42 signal ratio for individual animals visualized as superimposed plaque subtyped (diffuse and cored), grouped by age, demonstrated (E.I) the Aβ1-40/Aβ1-42 signal ratio in 12-month-old MO cortical plaques (orange) to be intermediate to that of diffuse plaques (yellow) and cored (green) plaques, respectively, in 18- and 23-month-old mice. As shown in the sample single ion images, the Aβ1-40/Aβ1-42 signal ratio was significantly higher for cored (green) as compared to diffuse (yellow) for all ages in all of (E.I) MO cortex, (E.II) HIP, and (E.III) SS cortex ($p<0.01$). No plaques were consistently found in HIP and SS cortex of 12-month-old animals. Nr of animals per group at 18, 23mo.: n=3/timepoint. Nr of plaques for each subtype, and animal: 10-15 plaques. Univariate comparisons of the peak data between the groups was performed using paired, two tailed t-test..Errorbars indicate SD. Scale bars A-D: 50 µm

Figure 6. Aggregation of C-terminal Aβ truncations.
Overlay images of the Aβ1-40 and Aβ1-42 peptide signal (as shown in Figure 4D) showed and intermediate mix of both peptides in plaque of a (A.I) 12-month-old mice.

A clear predominance of Aβ1-40 peptide was seen in (A.II, A.IV) cored plaques and for Aβ1-42 in (A.III, A.V) diffuse plaques in 18- and 23-month-old mice. Single ion images of (B.I-V) Aβ1-40, (C.I-V) Aβ1-39, (D.I-V) Aβ1-38, and (E.I-V) Aβ1-37 for the respective plaque types and mice ages listed above.

The different species displayed a varied colocalization of (B.I, C.I, D.I, E.I) in MO cortex plaques of 12-month-old mice, as well as (B.IV, C.IV, D.IV, E.IV) cored plaques in 23-month-old mice. Interestingly, in difference to the Aβ1-39 and Aβ1-37, Aβ1-38 peptide showed consistent colocalization with Aβ1-40, as in the cored plaques both in 18 months (B.II, D.II) and 23-month-old animals (B.IV, D.IV).

Bar plots for (F.I-III) Aβ1-39, (G.I-III) and Aβ1-38 relative signal intensity, showed a clearly higher signal of these peptides in the (green) cored plaques as compared to (yellow) diffuse plaque subtype. For the (F.I-III) Aβ1-39 this difference was significant for all regions in 23-month-old animals, as well as in the MO cortex of the 18-month-old mice ($p<0.05$).

(G.I-III) Aβ1-38 was consistently, significantly higher in cored plaques in all regions for both the 18-, and 23-month old animals ($p<0.05$). In contrast, Aβ1-37 (H.I-III) was not significantly different between plaque subpopulation across ages and regions, even though a higher relative signal intensity was observed in the cored deposits.

Correlation plots of (F.IV, V) Aβ1-39 vs Aβ1-40, (G.IV, V) Aβ1-38 vs Aβ1-40, (H.IV, V) Aβ1-37 vs Aβ1-40, among (green-left) cored plaques, and (yellow-right) diffuse plaques. Here, a clear correlation was observed between (F.IV) Aβ1-39 and Aβ1-40 among cored plaques ($R^2=0.4007$, $p < 0.005$), as well as between Aβ1-38 and Aβ1-40 among both (G.IV) cored plaques ($R^2=0.4978$, $p < 0.005$), and diffuse plaques ($R^2=0.3449$, $p <0.05$). Nr of animals per group at 18, 23mo.: n=3/timepoint. Nr of plaques for each subtype, and animal: 10-15 plaques. Univariate comparisons of the peak data between the groups was performed using paired, two tailed t-test. Errorbars indicate SD. Scale bars A-E: 50μm

References

Ahmed, M., Davis, J., Aucoin, D., Sato, T., Ahuja, S., Aimoto, S., Elliott, J. I., Van Nostrand, W. E. and Smith, S. O. (2010) Structural conversion of neurotoxic amyloid-beta(1-42) oligomers to fibrils. *Nature structural & molecular biology,* **17,** 561-567.

Bitan, G., Kirkitadze, M. D., Lomakin, A., Vollers, S. S., Benedek, G. B. and Teplow, D. B. (2003) Amyloid beta -protein (Abeta) assembly: Abeta 40 and Abeta 42 oligomerize through distinct pathways. *Proceedings of the National Academy of Sciences of the United States of America,* **100,** 330-335.

Braak, H. and Braak, E. (1991) Neuropathological staging of Alzheimer related changes *Acta Neuropathol,* **82,** 239-259.

Brinkmalm, G., Portelius, E., Ohrfelt, A. et al. (2012) An online nano-LC-ESI-FTICR-MS method for comprehensive characterization of endogenous fragments from amyloid beta and amyloid precursor protein in human and cat cerebrospinal fluid. *Journal of mass spectrometry : JMS,* **47,** 591-603.

Carlred, L., Michno, W., Kaya, I., Sjovall, P., Syvanen, S. and Hanrieder, J. (2016) Probing amyloid-beta pathology in transgenic Alzheimer's disease (tgArcSwe) mice using MALDI imaging mass spectrometry. *Journal of neurochemistry,* **138,** 469-478.

Chen, W., Gamache, E., Rosenman, D. J., Xie, J., Lopez, M. M., Li, Y. M. and Wang, C. (2014) Familial Alzheimer's mutations within APPTM increase Abeta42 production by enhancing accessibility of epsilon-cleavage site. *Nat Commun,* **5,** 3037.

Czirr, E., Cottrell, B. A., Leuchtenberger, S. et al. (2008) Independent generation of Abeta42 and Abeta38 peptide species by gamma-secretase. *The Journal of biological chemistry,* **283,** 17049-17054.

Esbjorner, E. K., Chan, F., Rees, E., Erdelyi, M., Luheshi, L. M., Bertoncini, C. W., Kaminski, C. F., Dobson, C. M. and Kaminski Schierle, G. S. (2014) Direct observations of amyloid beta self-assembly in live cells provide insights into differences in the kinetics of Abeta(1-40) and Abeta(1-42) aggregation. *Chemistry & biology,* **21,** 732-742.

Funamoto, S., Morishima-Kawashima, M., Tanimura, Y., Hirotani, N., Saido, T. C. and Ihara, Y. (2004) Truncated carboxyl-terminal fragments of beta-amyloid precursor protein are processed to amyloid beta-proteins 40 and 42. *Biochemistry,* **43,** 13532-13540.

Games, D., Adams, D., Alessandrini, R. et al. (1995) Alzheimer-type neuropathology in transgenic mice overexpressing V717F beta-amyloid precursor protein. *Nature,* **373,** 523-527.

Hanrieder, J., Ljungdahl, A., Falth, M., Mammo, S. E., Bergquist, J. and Andersson, M. (2011) L-DOPA-induced dyskinesia is associated with regional increase of striatal dynorphin peptides as elucidated by imaging mass spectrometry. *Molecular & cellular proteomics : MCP,* **10,** M111.009308.

Hanrieder, J., Malmberg, P. and Ewing, A. G. (2015) Spatial neuroproteomics using imaging mass spectrometry. *Biochimica et biophysica acta,* **1854,** 718-731.

Hanrieder, J., Malmberg, P., Lindberg, O. R., Fletcher, J. S. and Ewing, A. G. (2013) Time-of-flight secondary ion mass spectrometry based molecular histology of human spinal cord tissue and motor neurons. *Analytical chemistry,* **85,** 8741-8748.

Hardy, J. A. and Higgins, G. A. (1992) ALZHEIMERS-DISEASE - THE AMYLOID CASCADE HYPOTHESIS. *Science,* **256,** 184-185.

Higgins, L. S., Holtzman, D. M., Rabin, J., Mobley, W. C. and Cordell, B. (1994) Transgenic mouse brain histopathology resembles early Alzheimer's disease. *Ann Neurol,* **35,** 598-607.

Howlett, D. R. (2011) APP transgenic mice and their application to drug discovery. *Histology and histopathology,* **26,** 1611-1632.

Hsiao, K., Chapman, P., Nilsen, S., Eckman, C., Harigaya, Y., Younkin, S., Yang, F. and Cole, G. (1996) Correlative memory deficits, Abeta elevation, and amyloid plaques in transgenic mice. *Science,* **274,** 99-102.

Hsiao, K. K., Borchelt, D. R., Olson, K. et al. (1995) Age-related CNS disorder and early death in transgenic FVB/N mice overexpressing Alzheimer amyloid precursor proteins. *Neuron,* **15,** 1203-1218.

Ikeda, S., Allsop, D. and Glenner, G. G. (1989) A study of the morphology and distribution of amyloid beta protein immunoreactive plaque and related lesions in the brains of Alzheimer's disease and adult Down's syndrome. *Progress in clinical and biological research,* **317,** 313-323.

Iwatsubo, T., Odaka, A., Suzuki, N., Mizusawa, H., Nukina, N. and Ihara, Y. (1994) Visualization of A beta 42(43) and A beta 40 in senile plaques with end-specific A beta monoclonals: evidence that an initially deposited species is A beta 42(43). *Neuron,* **13,** 45-53.

Kakuda, N., Miyasaka, T., Iwasaki, N., Nirasawa, T., Wada-Kakuda, S., Takahashi-Fujigasaki, J., Murayama, S., Ihara, Y. and Ikegawa, M. (2017) Distinct deposition of amyloid-beta species in brains with Alzheimer's disease pathology visualized with MALDI imaging mass spectrometry. *Acta Neuropathol Commun,* **5,** 73.

Kawarabayashi, T., Younkin, L. H., Saido, T. C., Shoji, M., Ashe, K. H. and Younkin, S. G. (2001) Age-dependent changes in brain, CSF, and plasma amyloid (beta) protein in the Tg2576 transgenic mouse model of Alzheimer's disease. *J Neurosci,* **21,** 372-381.

Kaya, I., Brinet, D., Michno, W., Baskurt, M., Zetterberg, H., Blenow, K. and Hanrieder, J. (2017) Novel Trimodal MALDI Imaging Mass Spectrometry (IMS3) at 10 mum Reveals Spatial Lipid and Peptide Correlates Implicated in Abeta Plaque Pathology in Alzheimer's Disease. *ACS chemical neuroscience,* **8,** 2778-2790.

Klingstedt, T., Aslund, A., Simon, R. A., Johansson, L. B., Mason, J. J., Nystrom, S., Hammarstrom, P. and Nilsson, K. P. (2011) Synthesis of a library of oligothiophenes and their utilization as

fluorescent ligands for spectral assignment of protein aggregates. *Org Biomol Chem,* **9,** 8356-8370.

Kuo, Y. M., Beach, T. G., Sue, L. I. et al. (2001) The evolution of A beta peptide burden in the APP23 transgenic mice: implications for A beta deposition in Alzheimer disease. *Mol Med,* **7,** 609-618.

Lemere, C. A., Blusztajn, J. K., Yamaguchi, H., Wisniewski, T., Saido, T. C. and Selkoe, D. J. (1996) Sequence of deposition of heterogeneous amyloid beta-peptides and APO E in Down syndrome: implications for initial events in amyloid plaque formation. *Neurobiology of disease,* **3,** 16-32.

Lord, A., Kalimo, H., Eckman, C., Zhang, X.-Q., Lannfelt, L. and Nilsson, L. N. G. (2006) The Arctic Alzheimer mutation facilitates early intraneuronal Aβ aggregation and senile plaque formation in transgenic mice. *Neurobiology of Aging,* **27,** 67-77.

Lord, A., Philipson, O., Klingstedt, T., Westermark, G., Hammarstrom, P., Nilsson, K. P. and Nilsson, L. N. (2011) Observations in APP bitransgenic mice suggest that diffuse and compact plaques form via independent processes in Alzheimer's disease. *Am J Pathol,* **178,** 2286-2298.

Masters, C. L., Simms, G., Weinman, N. A., Multhaup, G., McDonald, B. L. and Beyreuther, K. (1985) Amyloid plaque core protein in Alzheimer disease and Down syndrome. *Proceedings of the National Academy of Sciences of the United States of America,* **82,** 4245-4249.

Matsumura, N., Takami, M., Okochi, M., Wada-Kakuda, S., Fujiwara, H., Tagami, S., Funamoto, S., Ihara, Y. and Morishima-Kawashima, M. (2014) gamma-Secretase associated with lipid rafts: multiple interactive pathways in the stepwise processing of beta-carboxyl-terminal fragment. *The Journal of biological chemistry,* **289,** 5109-5121.

McDonnell, L. A. and Heeren, R. M. (2007) Imaging mass spectrometry. *Mass spectrometry reviews,* **26,** 606-643.

McGowan, E., Pickford, F., Kim, J. et al. (2005) Abeta42 is essential for parenchymal and vascular amyloid deposition in mice. *Neuron,* **47,** 191-199.

Michno, W., Kaya, I., Nystrom, S., Guerard, L., Nilsson, K. P. R., Hammarstrom, P., Blennow, K., Zetterberg, H. and Hanrieder, J. (2018a) Multimodal Chemical Imaging of Amyloid Plaque Polymorphism Reveals Abeta Aggregation Dependent Anionic Lipid Accumulations and Metabolism. *Anal Chem,* **90,** 8130-8138.

Michno, W., Nystrom, S., Wehrli, P. et al. (2019) Pyroglutamation of amyloid-betax-42 (Abetax-42) followed by Abeta1-40 deposition underlies plaque polymorphism in progressing Alzheimer's disease pathology. *The Journal of biological chemistry*.

Michno, W., Wehrli, P. M., Blennow, K., Zetterberg, H. and Hanrieder, J. (2018b) Molecular imaging mass spectrometry for probing protein dynamics in neurodegenerative disease pathology. *Journal of neurochemistry*.

Nisbet, R. M., Polanco, J.-C., Ittner, L. M. and Götz, J. (2015) Tau aggregation and its interplay with amyloid-β. *Acta Neuropathol,* **129,** 207-220.

Nunan, J. and Small, D. H. (2000) Regulation of APP cleavage by alpha-, beta- and gamma-secretases. *FEBS Lett,* **483,** 6-10.

Nystrom, S., Psonka-Antonczyk, K. M., Ellingsen, P. G. et al. (2013) Evidence for age-dependent in vivo conformational rearrangement within Abeta amyloid deposits. *ACS Chem Biol,* **8,** 1128-1133.

Page, R. M., Baumann, K., Tomioka, M. et al. (2008) Generation of Abeta38 and Abeta42 is independently and differentially affected by familial Alzheimer disease-associated presenilin mutations and gamma-secretase modulation. *The Journal of biological chemistry,* **283,** 677-683.

Pannee, J., Portelius, E., Minthon, L., Gobom, J., Andreasson, U., Zetterberg, H., Hansson, O. and Blennow, K. (2016) Reference measurement procedure for CSF amyloid beta (Abeta)1-42 and the CSF Abeta1-42 /Abeta1-40 ratio - a cross-validation study against amyloid PET. *Journal of neurochemistry,* **139,** 651-658.

Philipson, O., Hammarstrom, P., Nilsson, K. P. et al. (2009) A highly insoluble state of Abeta similar to that of Alzheimer's disease brain is found in Arctic APP transgenic mice. *Neurobiol Aging,* **30,** 1393-1405.

Portelius, E., Tran, A. J., Andreasson, U., Persson, R., Brinkmalm, G., Zetterberg, H., Blennow, K. and Westman-Brinkmalm, A. (2007) Characterization of amyloid beta peptides in cerebrospinal fluid by an automated immunoprecipitation procedure followed by mass spectrometry. *Journal of proteome research,* **6,** 4433-4439.

Quon, D., Wang, Y., Catalano, R., Scardina, J. M., Murakami, K. and Cordell, B. (1991) Formation of beta-amyloid protein deposits in brains of transgenic mice. *Nature,* **352,** 239-241.

Rasmussen, J., Mahler, J., Beschorner, N. et al. (2017) Amyloid polymorphisms constitute distinct clouds of conformational variants in different etiological subtypes of Alzheimer's disease.

Proceedings of the National Academy of Sciences of the United States of America, **114,** 13018-13023.

Reinert, J., Martens, H., Huettenrauch, M. et al. (2014) Abeta38 in the brains of patients with sporadic and familial Alzheimer's disease and transgenic mouse models. *J Alzheimers Dis,* **39,** 871-881.

Reinert, J., Richard, B. C., Klafki, H. W. et al. (2016) Deposition of C-terminally truncated Abeta species Abeta37 and Abeta39 in Alzheimer's disease and transgenic mouse models. *Acta Neuropathol Commun,* **4,** 24.

Rohner, T. C., Staab, D. and Stoeckli, M. (2005) MALDI mass spectrometric imaging of biological tissue sections. *Mech Ageing Dev,* **126,** 177-185.

Saido, T. C., Iwatsubo, T., Mann, D. M., Shimada, H., Ihara, Y. and Kawashima, S. (1995) Dominant and differential deposition of distinct beta-amyloid peptide species, A beta N3(pE), in senile plaques. *Neuron,* **14,** 457-466.

Seeley, E. H. and Caprioli, R. M. (2008) Molecular imaging of proteins in tissues by mass spectrometry. *Proceedings of the National Academy of Sciences,* **105,** 18126-18131.

Seeley, E. H., Oppenheimer, S. R., Mi, D., Chaurand, P. and Caprioli, R. M. (2008) Enhancement of protein sensitivity for MALDI imaging mass spectrometry after chemical treatment of tissue sections. *Journal of the American Society for Mass Spectrometry,* **19,** 1069-1077.

Stoeckli, M., Knochenmuss, R., McCombie, G., Mueller, D., Rohner, T., Staab, D. and Wiederhold, K.-H. (2006) MALDI MS imaging of amyloid. *Methods Enzymol,* **412,** 94-106.

Sturchler-Pierrat, C., Abramowski, D., Duke, M. et al. (1997) Two amyloid precursor protein transgenic mouse models with Alzheimer disease-like pathology. *Proceedings of the National Academy of Sciences of the United States of America,* **94,** 13287-13292.

Thal, D. R., Rub, U., Orantes, M. and Braak, H. (2002) Phases of A beta-deposition in the human brain and its relevance for the development of AD. *Neurology,* **58,** 1791-1800.

Tycko, R. (2015) Amyloid polymorphism: structural basis and neurobiological relevance. *Neuron,* **86,** 632-645.

Wittnam, J. L., Portelius, E., Zetterberg, H. et al. (2012) Pyroglutamate amyloid beta (Abeta) aggravates behavioral deficits in transgenic amyloid mouse model for Alzheimer disease. *J Biol Chem,* **287,** 8154-8162.

Yang, J. and Caprioli, R. M. (2011) Matrix Sublimation/Recrystallization for Imaging Proteins by Mass Spectrometry at High Spatial Resolution. *Analytical chemistry,* **83,** 5728-5734.

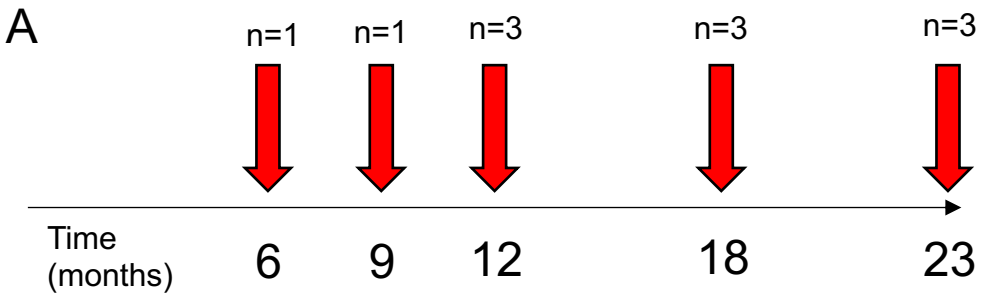

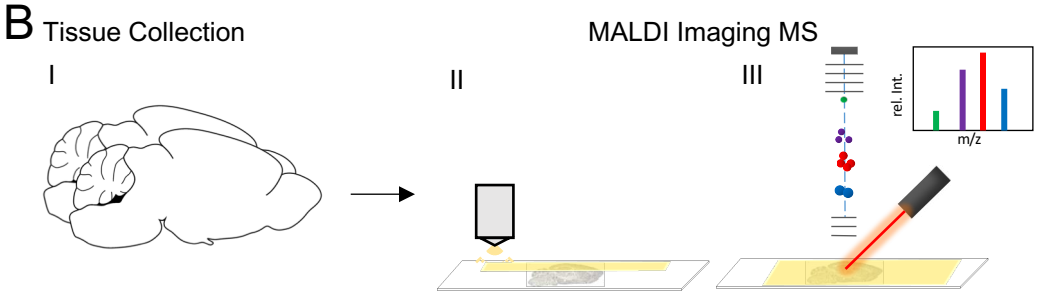

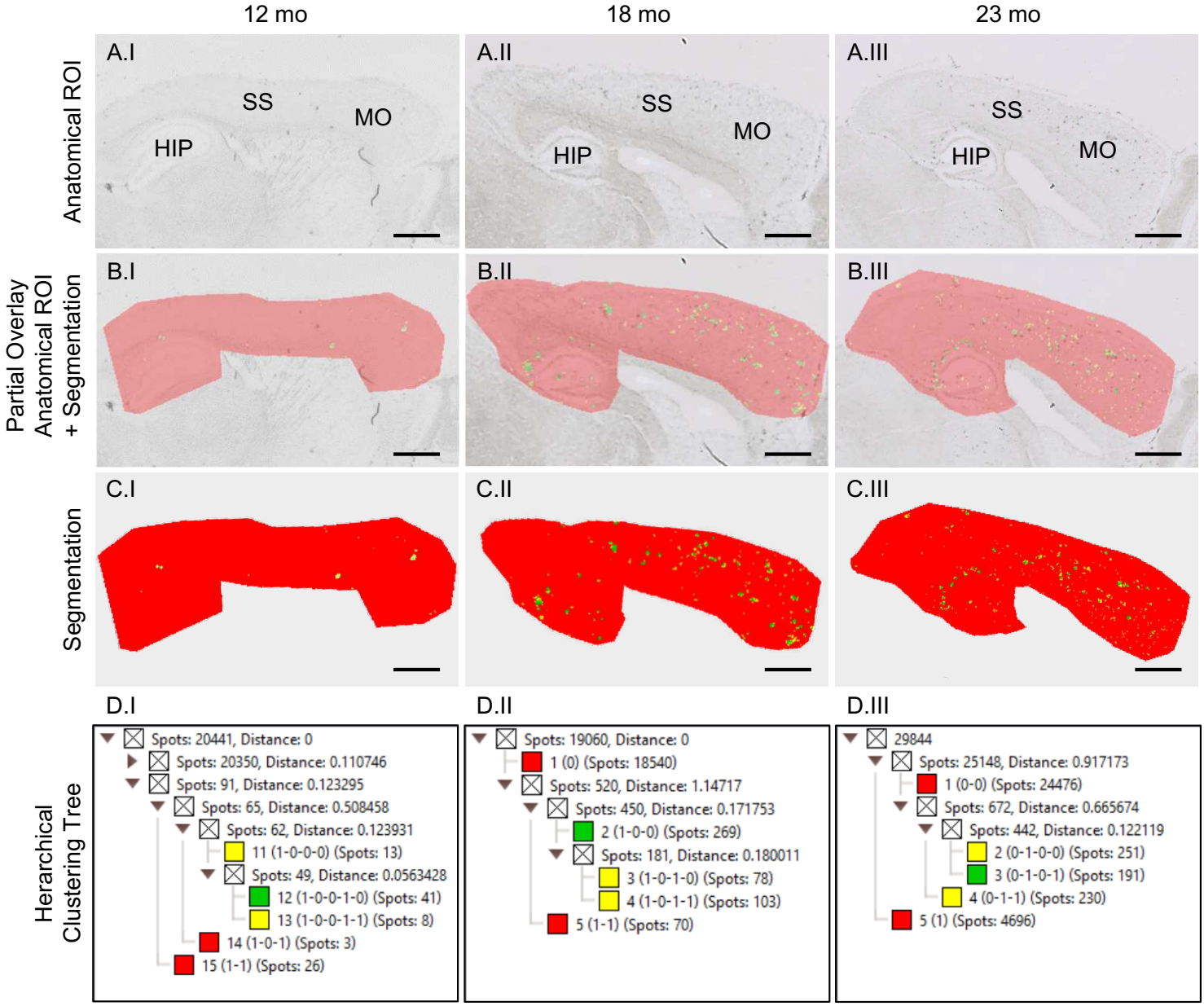
12 mo
18 mo
23 mo
Anatomical ROI
Partial Overlay Anatomical ROI + Segmentation
Segmentation
Herarchical Clustering Tree
A.I
A.II
A.III
SS
MO
HIP
B.I
B.II
B.III
C.I
C.II
C.III
D.I
Spots: 20441, Distance: 0
Spots: 20350, Distance: 0.110746
Spots: 91, Distance: 0.123295
Spots: 65, Distance: 0.508458
Spots: 62, Distance: 0.123931
11 (1-0-0-0) (Spots: 13)
Spots: 49, Distance: 0.0563428
12 (1-0-0-1-0) (Spots: 41)
13 (1-0-0-1-1) (Spots: 8)
14 (1-0-1) (Spots: 3)
15 (1-1) (Spots: 26)
D.II
Spots: 19060, Distance: 0
1 (0) (Spots: 18540)
Spots: 520, Distance: 1.14717
Spots: 450, Distance: 0.171753
2 (1-0-0) (Spots: 269)
Spots: 181, Distance: 0.180011
3 (1-0-1-0) (Spots: 78)
4 (1-0-1-1) (Spots: 103)
5 (1-1) (Spots: 70)
D.III
29844
Spots: 25148, Distance: 0.917173
1 (0-0) (Spots: 24476)
Spots: 672, Distance: 0.665674
Spots: 442, Distance: 0.122119
2 (0-1-0-0) (Spots: 251)
3 (0-1-0-1) (Spots: 191)
4 (0-1-1) (Spots: 230)
5 (1) (Spots: 4696)

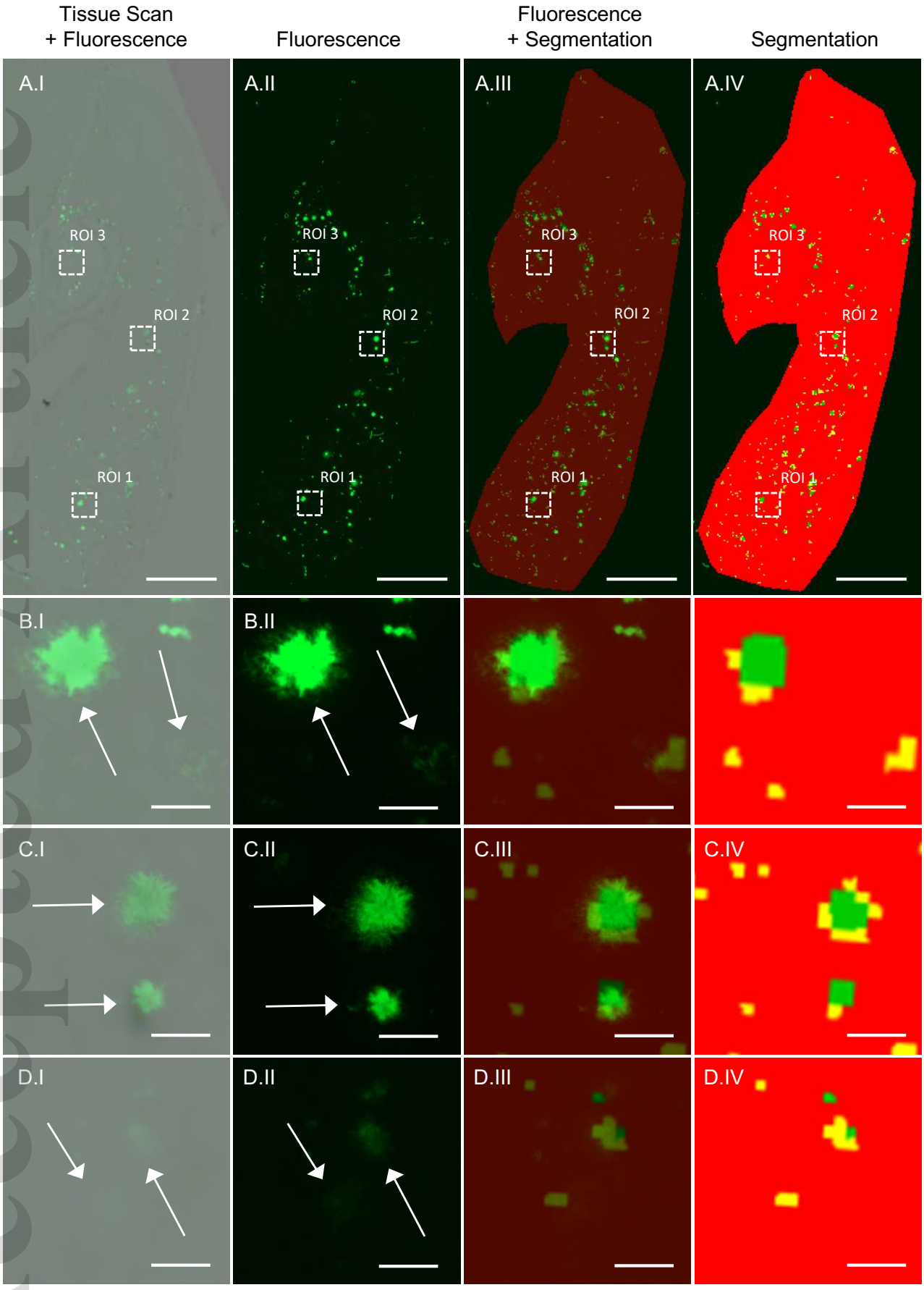

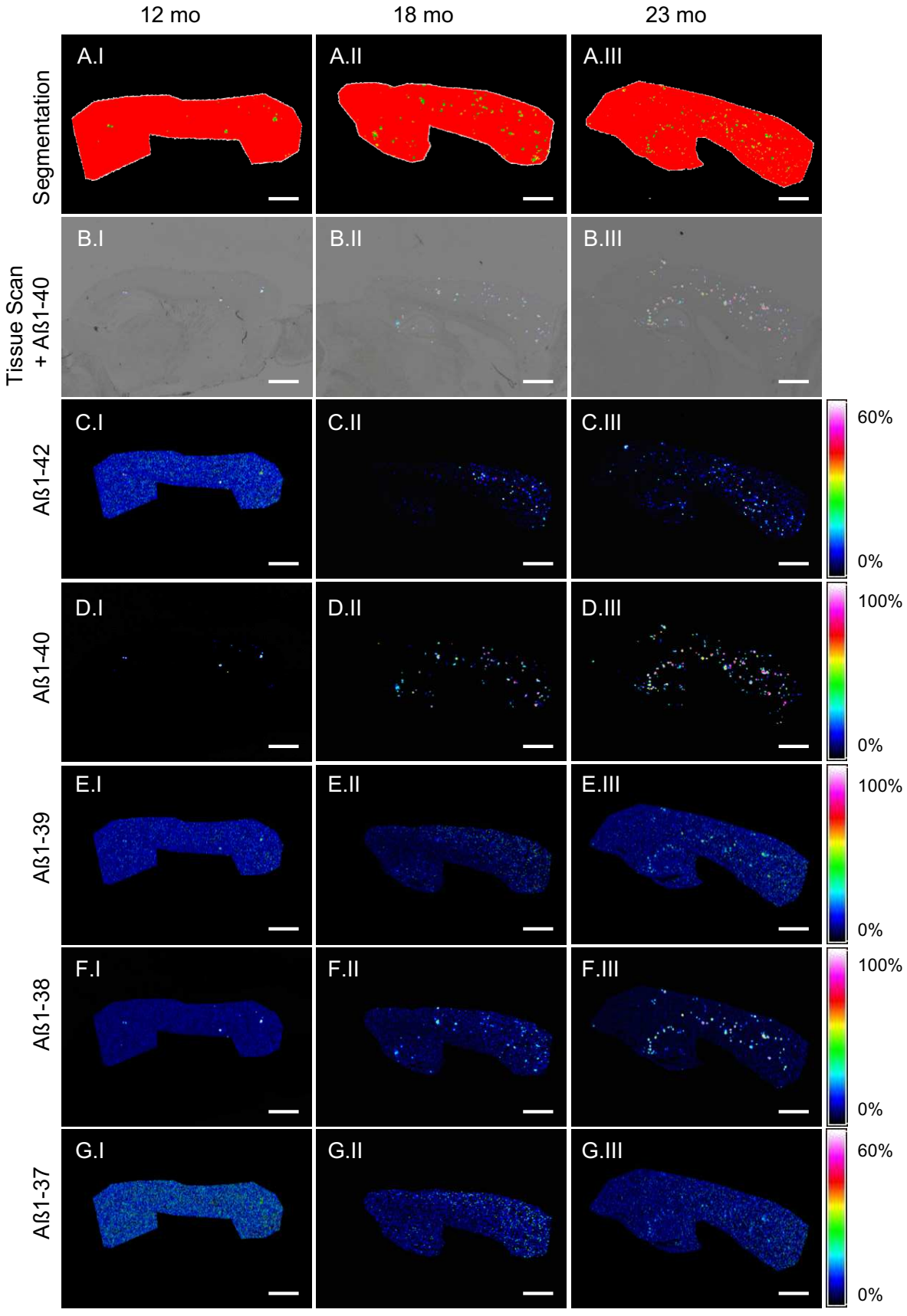

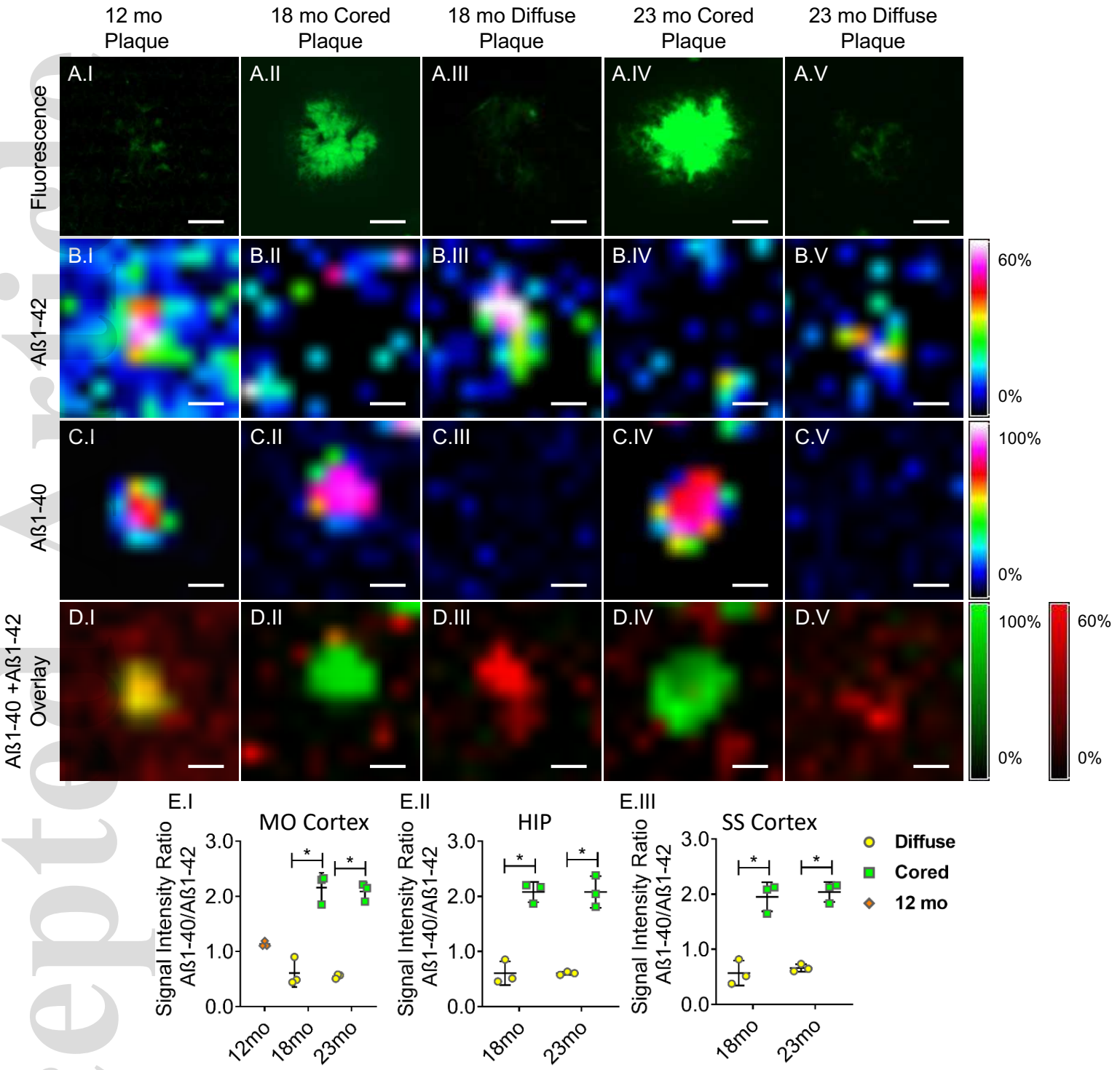

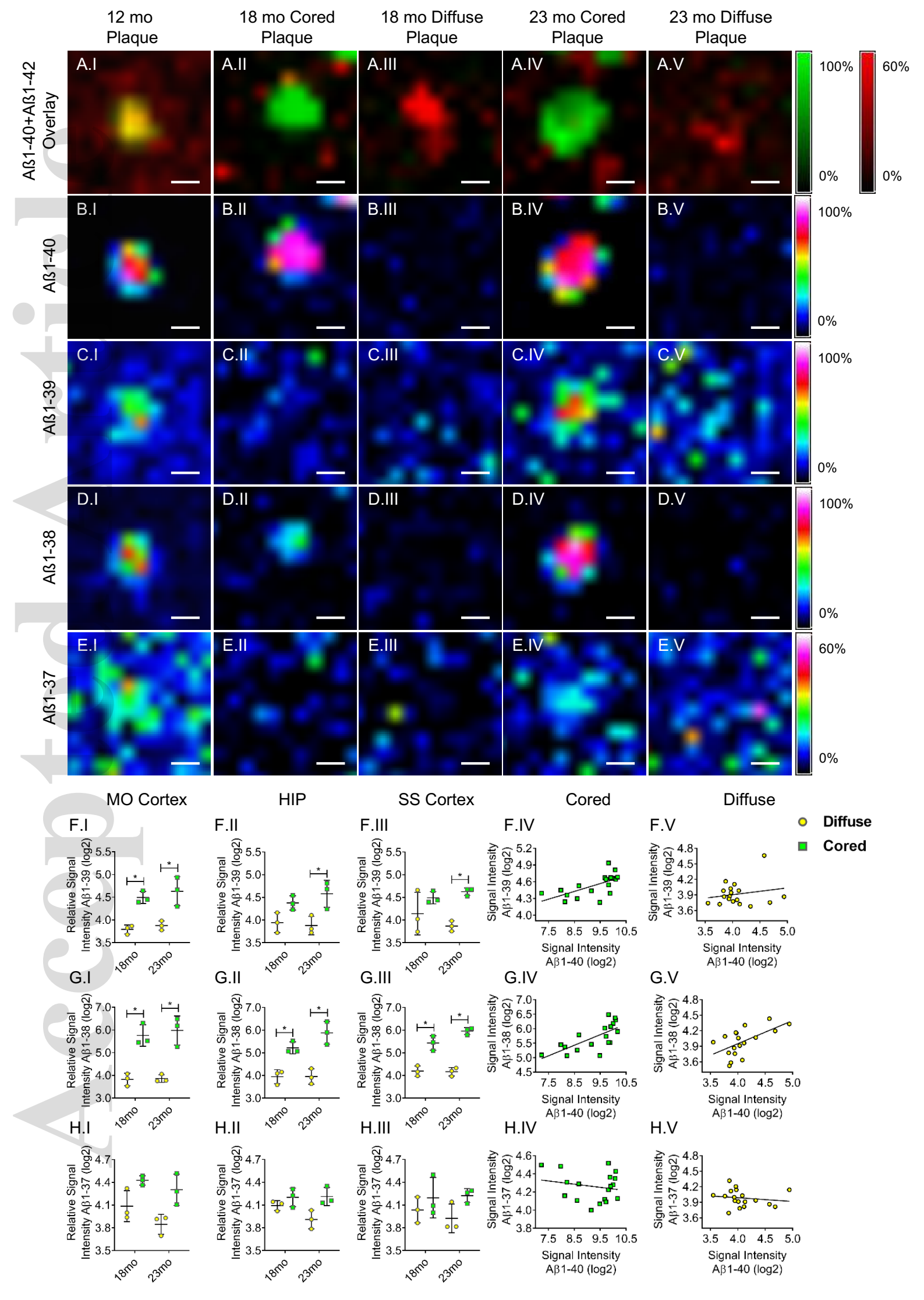
12 mo Plaque
18 mo Cored Plaque
18 mo Diffuse Plaque
23 mo Cored Plaque
23 mo Diffuse Plaque
Aß1-40+Aß1-42 Overlay
Aß1-40
Aß1-39
Aß1-38
Aß1-37
100%
0%
60%
MO Cortex
HIP
SS Cortex
Cored
Diffuse
Relative Signal Intensity Aβ1-39 (log2)
Relative Signal Intensity Aβ1-38 (log2)
Relative Signal Intensity Aβ1-37 (log2)
Signal Intensity Aβ1-39 (log2)
Signal Intensity Aβ1-38 (log2)
Signal Intensity Aβ1-37 (log2)
Signal Intensity Aβ1-40 (log2)
18mo
23mo
Diffuse
Cored